Title

Axial mechanical and structural characterization of keratoconus corneas

Authors

Mikula, Eric
Winkler, Moritz
Juhasz, Tibor
et al.

Publication Date

2018-10-01

DOI

10.1016/j.exer.2018.05.019

Peer reviewed

HHS Public Access

Author manuscript

Exp Eye Res. Author manuscript; available in PMC 2020 June 29.

Published in final edited form as:

Exp Eye Res. 2018 October ; 175: 14–19. doi:10.1016/j.exer.2018.05.019.

Axial mechanical and structural characterization of keratoconus corneas

Eric Mikula[a], **Moritz Winkler**[b], **Tibor Juhasz**[a,b], **Donald J. Brown**[a,b], **Golroxan Shoa**[a], **Stephanie Tran**[a], **M. Cristina Kenney**[a], **James V. Jester**[a,b,*]

[a]Gavin Herbert Eye Institute, Department of Ophthalmology, University of California, Irvine, CA, United States

[b]Department of Biomedical Engineering, University of California, Irvine, CA, United States

Abstract

Purpose: Previous studies indicate that there is an axial gradient of collagen lamellar branching and anastomosing leading to regional differences in corneal tissue stiffness that may control corneal shape. To further test this hypothesis we have measured the axial material stiffness and quantified the collagen lamellar complexity in ectatic and mechanically weakened keratoconus corneas (KC).

Methods: Acoustic radiation force elastic microscopy (ARFEM) was used to probe the axial mechanical properties of the cone region of three donor KC buttons. 3 Dimensional second harmonic generation microscopy (3D-SHG) was used to qualitatively evaluate lamellar organization in 3 kC buttons and quantitatively measure lamellar branching point density (BPD) in a separate KC button that had been treated with epikeratophakia (Epi-KP).

Results: The mean elastic modulus for the KC corneas was 1.67 ± 0.44 kPa anteriorly and 0.970 ± 0.30 kPa posteriorly, substantially below that previously measured for normal human cornea. 3D-SHG of KC buttons showed a simplified collagen lamellar structure lacking noticeable angled lamellae in the region of the cone. BPD in the anterior, posterior, central and paracentral regions of the KC cornea were significantly lower than in the overlying Epi-KP lenticule. Additionally, BPD in the cone region was significantly lower than the adjacent paracentral region in the KC button.

Conclusions: The KC cornea exhibits an axial gradient of mechanical stiffness and a BPD that appears substantially lower in the cone region compared to normal cornea. The findings reinforce the hypothesis that collagen architecture may control corneal mechanical stiffness and hence corneal shape.

1. Introduction

Keratoconus (KC) affects roughly 1 in 2000 people and is characterized by progressive paracentral corneal thinning and steepening (Rabinowitz, 1998). As a result, the cornea takes on a conical shape leading to myopia, astigmatism, and markedly reduced visual acuity. The

*Corresponding author. 843 Health Sciences Road, Hewitt Hall, Room 2036, University of California, Irvine, Irvine, CA, 92697-4390, United States. jjester@uci.edu (J.V. Jester).

onset of keratoconus typically occurs in childhood to early adulthood and progresses before stabilizing by the fourth decade (Gordon-Shaag et al., 2015; Bykhovskaya et al., 2016). The pathogenesis of KC is commonly accepted to involve both environmental and genetic factors, with environmental factors possibly acting as triggers for the condition in genetically predisposed individuals. Among environmental factors are eye rubbing, atopy, and UV exposure, while genome wide association studies (GWAS) and genome wide linkage studies (GWLS) have identified numerous genes related to KC (Gordon-Shaag et al., 2015; Bykhovskaya et al., 2016). Regardless of the specific pathogenesis, abnormal collagen structure in the KC cornea is thought to weaken overall mechanical properties thus resulting in the formation of the hallmark cone in response to intraocular pressure (IOP).

The healthy human cornea possesses a unique collagen structure, which has been proposed to play a key role in the maintenance of corneal shape, biomechanics, and in turn visual acuity (Winkler et al., 2013; Kling and Hafezi, 2017). 3-dimensional second harmonic generation imaging (3D-SHG) has shown that lamellae in the anterior cornea branch and anastomose with one another and run at oblique angles relative to Bowman's layer, while in the posterior cornea, lamellae run parallel to the anterior and posterior limiting lamina with significantly reduced branching (Jester et al., 2010; Winkler et al., 2011; Winkler et al., 2013). It has also been established that there are bow spring fibers which extend from Bowman's layer and intertwine with deeper fibers (Morishige et al., 2011; Winkler et al., 2011; Mercatelli et al., 2017). Recent studies have also shown that these structural differences are associated with distinctly different mechanical properties in the cornea leading to increased mechanical stiffness and elastic modulus in the anterior cornea that is two to three fold higher than the posterior cornea (Winkler et al., 2011; Petsche et al., 2012; Dias et al., 2013; Dias and Ziebarth, 2013; Mikula et al., 2016). The KC cornea stands in stark contrast to the healthy cornea, both in regard to mechanics (Andreassen et al. 1980; Edmund 1988, 1989; Scarcelli, Besner et al. 2014, 2015) as well as collagen structure (Meek et al., 2005; Morishige et al., 2007; Morishige, Shin-gyou-uchi et al., 2014). Specifically, Morishige et al. have shown that collagen structure varies axially in the KC cornea when compared to the healthy cornea (Morishige et al., 2007; Morishige, Shin-gyou-uchi et al., 2014). Given that collagen structure is inextricably tied to biomechanical properties and that KC structure from anterior to posterior varies significantly compared to healthy corneas, it is expected that biomechanical properties will also vary in the axial direction.

The primary objective of this study was to assess the axial variation in mechanical properties of keratoconic corneal buttons using acoustic radiation force elastic microscopy (ARFEM). For structural comparison to biomechanical results, collagen architecture was qualitatively evaluated in KC corneal buttons, and then quantitatively analyzed in KC button obtained from a patient that had received Epikeratophakia (Epi-KP) using 3D-SHG. The analysis of the Epi-KP button allowed for the assessment of lamellar collagen branching point density (BPD) in both the KC cornea and overlying Epi-KP lenticule, allowing for direct comparison in the same sample.

2. Materials and methods

All samples were procured with approval from the University of California, Irvine, the Institutional Review Board (UCI IRB #20054276), and in accordance with the Tenets of the Declaration of Helsinki. A total of 7 keratoconus (KC) buttons were used in this study that were obtained from the Gavin Herbert Eye Institute (UCI, Irvine, Ca). For ARFEM studies, 3 kC buttons were obtained on ice in Optisol immediately after surgery and stored at 4 °C; mechanical testing was performed within three days of KC surgery. For the SHG studies, the 4 kC buttons were immediately fixed in 4% paraformaldehyde in phosphate buffered saline (PBS), pH 7.2, and processed as discussed below. All samples were inspected under a stereomicroscope to qualitatively assess the state of the corneas with regards to swelling and transparency and to ensure the absence of any major visible defects or abnormalities.

2.1. Elasticity measurements using ARFEM

The ARFEM technique used in this study to evaluate biomechanics is described in detail elsewhere(Mikula et al., 2014). Briefly, a femtosecond laser pulse (Coherent, Inc., Santa Clara, CA) is used to create a microbubble in a corneal sample, which is embedded within 7.5% gelatin and precisely positioned within a sample chamber. A custom high-intensity, focused ultrasound (Resource Center for Medical Ultrasonic Transducer Technology, University of Southern California) displaces the microbubble axially within the cornea while low intensity acoustic pulse-echoes (A-scan) track the position of the bubble in time. The bubble is preconditioned with a series of 5 acoustic radiation force pulses, with the fifth being recorded for analysis. The maximum displacement of the bubble in response to the acoustic force is inversely proportional to the local elastic modulus. The measurements in the KC corneas were performed in the anterior and posterior portions of the central cone, which were defined as being within 100 μm of the anterior and posterior surfaces, respectively. The custom ARFEM system was chosen to axially evaluate corneal tissue elasticity due to its ability to non-destructively probe the tissue of interest at different depths without the need for mechanical sectioning, thus preserving the overall tissue structure. Biomechanical properties can be affected by tissue swelling, thus, care was taken to maintain cornea thickness (hydration) within a reasonable physiological range for ARFEM measurements.

2.2. Sample preparation and SHG imaging

The 4 kC buttons evaluated by SHG imaging were obtained immediately post surgery and comprised 3 buttons from 3 different patients that had no previous surgical interventions, and 1 button from a patient that had previously undergone epikeratophakia (Epi-KP) surgery at least 10 years prior to corneal transplant surgery. All samples were prepared following previously established methods and imaged using our standard nonlinear optical high resolution macroscopy (NLO-HRMac) protocol (Jester et al., 2010; Winkler et al., 2013). Briefly, samples were embedded vertically in low melting point agarose (Nu-Sieve GTG, Lonza Group Ltd., Rockland, ME) and 200 μm tissue sections were collected from the central, cone region of the button using a vibratome (Vibratome 1500; Intracel Ltd., Shepreth, UK). Tissue sections were stored in 4% PFA in PBS until imaged using second harmonic generation microscopy as described previously(Winkler et al., 2013). Briefly,

samples were placed on a glass slide under a laser scanning microscope (Zeiss 510 LSM; Carl Zeiss, Inc., Thornwood, NY) and illuminated with 76 MHz, 150 fs laser pulses from a femtosecond oscillator (Chameleon Titanium Sapphire laser; Coherent, Santa Clara, CA) tuned to 820 nm. The backscattered second harmonic signal (390–430 nm) was collected by the LSM's meta detector.

2.3. Quantification of collagen fiber branching

Using the 3D-SHG image data sets, individual collagen lamellae in the anterior region of the Epi-KP lenticule and in both the central (cone region) and adjacent, paracentral region of the host KC button were manually segmented using a highlighting tool in Amira 5.4.3 software (Visual Sciences Group, Burlington, MA). 3-D reconstructions of the fibers were chosen based on the vicinity of the cone to compare the different branching densities as a function of depth between the Epi-KP and keratoconic regions of the sample.

Branching point density (BDP) was quantified using previously published methodology (Winkler et al., 2011). Briefly, lines connecting the anterior and posterior surfaces and running perpendicular to Bowman's layer in both the Epi-KP lenticule and underlying KC button were drawn at 500 μm intervals from the central to paracentral cornea. These lines were then further subdivided with 8 equally spaced dividers through the depth of the sample. The Epi-KP lenticule was overlaid with 9 lines, each containing 8 dividers (~ 375 μm thickness), while KC button was assigned 6 lines, each containing 8 dividers (~ 500 μm thickness). The collagen fiber closest to a given divider was chosen and analyzed for branching density. The fiber was manually tracked in the software through the 3-D image stack to locate the two closest branching points of the fiber on either side of the line. The coordinates of the four branching points were logged into a spreadsheet (Microsoft Excel) and used to calculate the amount of branching points per millimeter at that particular depth.

For both the KC and Epi-KP lenticule portions of the sample, the BPD was calculated for 4 distinct axial and lateral regions: anterior, posterior, central, and paracentral. The anterior and posterior regions were defined as the anterior and posterior 100 microns spanning laterally across the sample from the central to the paracentral cornea. The central region was defined as the innermost 1 mm spanning axially from anterior to posterior through the full thickness of the sample. The paracentral region was defined as the outermost 1 mm spanning axially from anterior to posterior through the full thickness of the sample. Thus, the anterior and posterior statistics contain data from the entire lateral length of the sample, while the central and paracentral statistics contain data from the entire axial thickness of the sample.

2.4. Statistics

A student's t-test was used (Matlab, Natick, MA) to evaluate the difference in means between the elasticity in the anterior and posterior KC cornea. A one-way ANOVA employing the Newman-Keuls method was used to evaluate the difference in means between anterior, posterior, central, and paracentral regions in the KC and epikeratophakic lenticule.

3. Results

The elastic moduli for the anterior KC corneas as measured by ARFEM were 1.46 ± 0.23 kPa (Pa), 1.39 ± 0.51 kPa, and 2.17 ± 0.32 kPa. The elastic moduli for the posterior KC corneas were 0.94 ± 0.19 kPa, 0.68 ± 0.26 kPa, and 1.28 ± 0.63 kPa. The mean elastic modulus in the anterior region of the KC corneas (1.67 ± 0.44 kPa) was found to be significantly greater than the mean elastic modulus of the posterior region of the KC corneas (0.97 ± 0.30 kPa) ($p < 0.05$), while both were markedly less than reported for the normal cornea (Mikula et al., 2016). Fig. 1 summarizes the anterior/posterior elasticity measurements in the 3 kC corneas.

Figs. 2 and 3 are SHG backscatter images of two of the three KC buttons that were qualitatively evaluated to access lamellar complexity. As shown in the HR-Mac images covering most of the corneal button (Figs. 2A and 3A), the central region of the cone appears considerably thinner than the more peripheral region, and contains collagen lamellae oriented primarily parallel to the corneal surface. This is shown in greater detail in the 'zoomed' images (Figs. 2B and 3B) where the central cone region shows relatively flat collagen lamellae with little if any branching or anastomosing. This is in contrast to the regions immediately adjacent to the cone (Figs. 2C and 3C), where more normal anterior lamellae show obvious branching and anastomosing with many lamellae forming acute angles to the corneal surface.

Fig. 4 shows the HR-Mac SHG image of the Epi-KP button. 3-D reconstruction of collagen fibers in the anterior regions of the Epi-KP lenticule showed a marked difference to that observed in the KC cone region regarding collagen fiber branching and the presence of bow spring fibers attaching to the anterior limiting lamina (Bowman's layer). In the Epi-KP lenticule many bow spring fibers (teal) are apparent, which arc upward and insert into Bowman's layer (green) and then return to the anterior stroma where they show extensive branching and anastomosing (Fig. 5B). In comparison, Fig. 5C shows a marked loss of bow spring fibers and fiber branching within the cone region of the KC button. These structures, highlighted in magenta are nearly absent within cone region and appear to resemble smooth lines running nearly parallel to the curvature of Bowman's layer outlined in yellow (Fig. 5C). However, once outside of the cone region in the KC sample (Fig. 5D), bow spring fibers and fiber branching begin to reappear, although the apparent density remains below that observed in the Epi-KP lenticule.

Collagen fiber BPD in the host KC and Epi-KP lenticule were measured as a function of axial depth and the results presented in Fig. 5. The BPD's in the host KC cornea were 7.5 ± 3.4 mm^{-1} and 4.6 ± 2.3 mm^{-1} in the anterior and posterior, respectively. In the Epi-KP lenticule the BPD's were 12.0 ± 3.6 mm^{-1} and 6.9 ± 2.6 mm^{-1} in the anterior and posterior regions, respectively. This data indicated that the anterior and posterior BPD's in the Epi-KP lenticule were roughly 60% greater than that measured in the anterior and posterior KC cone regions, respectively ($p < 0.05$). BPD between the central and paracentral regions of the Epi-KP lenticule and KC cornea were also compared. The BPD's in the central (innermost 1 mm) and paracentral (outermost 1 mm) regions in the KC cornea were 4.4 ± 1.3 mm^{-1} and 6.6.± 3.0 mm^{-1}, respectively (Fig. 6), indicating that there was significantly more collagen

branching in the paracentral region of the KC cornea compared to the central cone ($p < 0.05$). The BPD's in the central and paracentral regions of the Epi-KP lenticule were 8.8 ± 2.8 mm^{-1} and 9.3 ± 4.1 mm^{-1}, respectively (Fig. 6). Overall, the Epi-KP lenticule had a significantly higher BPD than the KC cornea ($p = 0.001$). There was no statistical difference in BPD between the central and paracentral regions in the Epi-KP lenticule.

4. Discussion

The axial distribution of mechanical properties in the cone region of KC buttons was investigated using ARFEM along with BPD in a KC button obtained from a patient who had previously been treated with epikeratophakia to measure of collagen structural complexity. Additional KC corneas were imaged using SHG microscopy to qualitatively elucidate varying complexity in collagen architecture. Compared to published results also using ARFEM, the overall elastic modulus in the KC cornea is roughly half of that in the healthy cornea (Mikula et al., 2016), which is well established in the literature (Andreassen et al. 1980; Edmund 1988, 1989; Scarcelli, Besner et al. 2014, 2015). Brillouin elastic microscopy in the ex-vivo KC cornea has similarly shown a significant decrease in Brillouin modulus when compared to the healthy cornea (Scarcelli et al., 2014). Though Brillouin and Young's moduli are not measures of the same physical quantity and some research reports that Brillouin modulus is strongly correlated with hydration (Wu et al., 2017), experimental data point to a quantitative correlation between the two measurements (Scarcelli and Yun, 2007; Scarcelli et al., 2012; Scarcelli, Besner et al. 2014, 2015). Aside from questions regarding Brillouin elasticity measurements, the results provided in this study confirm these previous measurements and provide the first axial measurements of elasticity in the KC cornea. Interestingly, the decrease in elasticity seemed to equally effect the anterior and posterior cornea with the anterior cone being roughly 1.7x stiffer than the posterior ($p < 0.05$), a ratio similar to that detected in the normal cornea (Winkler et al., 2011; Last et al., 2012; Petsche et al., 2012; Scarcelli et al., 2012; Dias and Ziebarth, 2013; Winkler et al., 2013; Mikula et al., 2016). These findings suggest that the underlying mechanisms leading to the loss of mechanical strength in KC affect both the anterior and posterior cornea equally.

In addition to elastic data, our BPD measurements in the KC cornea revealed a significant reduction in BPD, or complexity, between the anterior and posterior KC cornea ($p < 0.05$), suggesting a link between collagen branching/interweaving and mechanical strength. The branching point density (BPD) of collagen fibers has been previously described as a metric for quantifying collagen interconnectivity in the cornea and is thought to be related to elastic modulus (Winkler et al., 2011). A recent study indicated a similar relationship between collagen structure and mechanics in the healthy cornea; the results showing that both the elastic modulus (as measured by indentation testing) and BPD decreased as a function of depth moving from the anterior to posterior cornea (Winkler et al., 2011). Another study revealed a similar relationship between structure and elasticity as evaluated by SHG imaging and atomic force microscopy in the rabbit cornea (Thomasy et al., 2014). Our study also found that the paracentral region adjacent to the cone in the KC button had a significantly higher BPD ($p < 0.001$) than in the KC cone region, indicating that the collagen architecture changes are most pronounced in the cone. Previous studies concerning collagen architecture in the KC and healthy cornea have shown similar trends. Morishige et al. showed that

interweaving among collagen lamellae is markedly diminished in the KC cornea compared to the healthy cornea, and that lamellar insertion into Bowman's layer is reduced or absent altogether (Morishige et al., 2007). Similarly, fast Fourier transform (FFT) analysis of SHG images revealed that the angle of sutural lamellae relative to Bowman's layer are significantly reduced in the KC cornea (Mercatelli et al., 2017). Both BPD and lamellar angle measurements reveal a similar trend in the keratoconic cornea and show that there is a disruption in the normal architecture, especially in the anterior segment. In addition to differences in collagen architecture between normal and KC corneas, there are also differences in microfibril bundle (MB) distribution between the normal and diseased state. In the KC cornea, there are less apparent MB's just anterior to Descemet's membrane while there is an increased number of MB's just beneath the epithelium; MB's just posterior to the epithelium are comparatively absent in the normal cornea. It is thought that the increased concentration of MB's beneath the epithelium in the KC cornea is a biomechanical response to strengthen the cone region (White et al., 2017).

It is also interesting to note that outside of the cone in the KC cornea there is a reappearance of bow spring fibers and an increase in interweaving, resembling healthy collagen architecture. This is similar to findings reporter by Radner et al. using scanning electron microscopy (Radner et al., 1998; Radner et al., 1998; Radner and Mallinger, 2002). They found interweaving between adjacent fibers was severely limited or absent altogether within the KC cone. Likewise, they found that outside of the cone the three-dimensional arrangement of collagen lamellae did not differ from normal corneas (Radner et al., 1998). Mechanically, Scarcelli et al. reported that the elasticity outside of the cone region in the KC cornea is significantly greater than within the cone, but not significantly different than the elasticity in a healthy cornea (Scarcelli et al., 2014). Similarly, the BPD in the central KC cone is significantly lower than in the paracentral region ($p < 0.05$), while there is no statistical difference between the central and paracentral BPD in the Epi-KP lenticule. Overall, there are obvious differences in the collagen structure of the KC cornea which seem to explain the overall mechanical weakness of the KC cornea, as well as the finding in this study that elastic modulus decreases as a function of depth in the KC cornea.

A potential drawback concerning this study was the inability to perform ARFEM measurements in the paracentral region of the KC buttons. Due to the fact that the KC samples were excised buttons and embedded in gelatin, the edges of the samples (paracentral) were subject to uncontrollable tissue swelling conditions that would render mechanical measurements unreliable at best. An additional drawback of the study is the lack of BPD measurements in more KC corneas. Unfortunately, BPD measurements are labor intensive but future studies might expand upon these interesting findings.

5. Conclusion

In this study it was found that the anterior KC cornea is roughly twice as stiff as the posterior KC cornea and that this may be related to depth dependent changes in collagen architecture. ARFEM elasticity measurements in the anterior and posterior KC cornea were compared against the collagen architecture of healthy and KC regions of an epikeratophakic sample, and also against a backscattered SHG images taken in KC buttons. There is a clear

reduction in interweaving in the KC cone region when compared to the healthy cornea, as well as a decrease in interweaving as a function of depth. The findings reinforce the hypothesis that specific structural elements such as transverse bow string fibers and dense lamellar interweaving, especially with respect to the anterior cornea, are associated with corneal elastic modulus. On a broader note, this study reinforces the important role of collagen structure in defining the form and function of the cornea. In the normal cornea, collagen lamellae are organized into a complex, intertwined network that provides the mechanical strength necessary to maintain corneal shape for the controlled refraction of light onto the retina. Alteration in collagen structure, as occurs in KC, leads to mechanical weakening of the cornea, alteration in corneal shape, and loss of visual function.

Acknowledgments

Funding

Supported in part by NEI EY024600 and EY018665, and an unrestricted grant from Research to Prevent Blindness, Inc. RPB-203478.

References

Andreassen TT, Hjorth Simonsen A, Oxlund H, 1980 Biomechanical properties of keratoconus and normal corneas. Exp. Eye Res 31 (4), 435–441. [PubMed: 7449878]

Bykhovskaya Y, Margines B, Rabinowitz YS, 2016 Genetics in Keratoconus: where are we? Eye Vis (Lond) 3, 16. [PubMed: 27350955]

Dias J, Diakonis VF, Kankariya VP, Yoo SH, Ziebarth NM, 2013 Anterior and posterior corneal stroma elasticity after corneal collagen crosslinking treatment. Exp. Eye Res 116, 58–62. [PubMed: 23933527]

Dias JM, Ziebarth NM, 2013 Anterior and posterior corneal stroma elasticity assessed using nanoindentation. Exp. Eye Res 115, 41–46. [PubMed: 23800511]

Edmund C, 1988 Corneal elasticity and ocular rigidity in normal and keratoconic eyes. Acta Ophthalmol. 66 (2), 134–140. [PubMed: 3389085]

Edmund C, 1989 Corneal topography and elasticity in normal and keratoconic eyes. A methodological study concerning the pathogenesis of keratoconus. Acta Ophthalmol. Suppl 193, 1–36. [PubMed: 2552742]

Gordon-Shaag A, Millodot M, Shneor E, Liu Y, 2015 The genetic and environmental factors for keratoconus. BioMed Res. Int 2015, 795738. [PubMed: 26075261]

Jester JV, Winkler M, Jester BE, Nien C, Chai D, Brown DJ, 2010a Evaluating corneal collagen organization using high-resolution nonlinear optical macroscopy. Eye Contact Lens 36 (5), 260–264. [PubMed: 20724856]

Jester JV, Winkler M, Jester BE, Nien C, Chai D, Brown DJ, 2010b Evaluating corneal collagen organization using high resolution non linear optical (NLO) macroscopy. Eye Contact Lens 36 (5), 260. [PubMed: 20724856]

Kling S, Hafezi F, 2017 Corneal biomechanics - a review. Ophthalmic Physiol. Optic 37 (3), 240–252.

Last JA, Thomasy SM, Croasdale CR, Russell P, Murphy CJ, 2012 Compliance profile of the human cornea as measured by atomic force microscopy. Micron 43 (12), 1293–1298. [PubMed: 22421334]

Meek KM, Tuft SJ, Huang Y, Gill PS, Hayes S, Newton RH, Bron AJ, 2005 Changes in collagen orientation and distribution in keratoconus corneas. Invest. Ophthalmol. Vis. Sci 46 (6), 1948–1956. [PubMed: 15914608]

Mercatelli R, Ratto F, Rossi F, Tatini F, Menabuoni L, Malandrini A, Nicoletti R, Pini R, Pavone FS, Cicchi R, 2017 Three-dimensional mapping of the orientation of collagen corneal lamellae in healthy and keratoconic human corneas using SHG microscopy. J. Biophot 10 (1), 75–83.

Mikula E, Hollman K, Chai D, Jester JV, Juhasz T, 2014 Measurement of corneal elasticity with an acoustic radiation force elasticity microscope. Ultrasound Med. Biol 40 (7), 1671–1679. [PubMed: 24726798]

Mikula ER, Jester JV, Juhasz T, 2016 Measurement of an elasticity map in the human cornea. Invest. Ophthalmol. Vis. Sci 57 (7), 3282–3286. [PubMed: 27327584]

Morishige N, Shin-gyou-uchi R, Azumi H, Ohta H, Morita Y, Yamada N, Kimura K, Takahara A, Sonoda K-H, 2014 Quantitative analysis of collagen lamellae in the normal and keratoconic human cornea by second harmonic generation imaging MicroscopyQuantitative analysis of collagen lamellae. Invest. Ophthalmol. Vis. Sci 55 (12), 8377–8385. [PubMed: 25425311]

Morishige N, Takagi Y, Chikama T, Takahara A, Nishida T, 2011 Three-dimensional analysis of collagen lamellae in the anterior stroma of the human cornea visualized by second harmonic generation imaging microscopy. Invest. Ophthalmol. Vis. Sci 52 (2), 911–915. [PubMed: 20881300]

Morishige N, Wahlert AJ, Kenney MC, Brown DJ, Kawamoto K, Chikama T, Nishida T, Jester JV, 2007 Second-harmonic imaging microscopy of normal human and keratoconus cornea. Invest. Ophthalmol. Vis. Sci 48 (3), 1087–1094. [PubMed: 17325150]

Petsche SJ, Chernyak D, Martiz J, Levenston ME, Pinsky PM, 2012 Depth-dependent transverse shear properties of the human corneal stroma. Invest. Ophthalmol. Vis. Sci 53 (2), 873. [PubMed: 22205608]

Rabinowitz YS, 1998 Keratoconus. Surv. Ophthalmol 42 (4), 297–319. [PubMed: 9493273]

Radner W, Mallinger R, 2002 Interlacing of collagen lamellae in the midstroma of the human cornea. Cornea 21 (6), 598–601. [PubMed: 12131038]

Radner W, Zehetmayer M, Aufreiter R, Mallinger R, 1998a Interlacing and cross-angle distribution of collagen lamellae in the human cornea. Cornea 17 (5), 537–543. [PubMed: 9756449]

Radner W, Zehetmayer M, Skorpik C, Mallinger R, 1998b Altered organization of collagen in the apex of keratoconus corneas. Ophthalmic Res. 30 (5), 327–332. [PubMed: 9704337]

Scarcelli G, Besner S, Pineda R, Kalout P, Yun S, 2015 IN vivo biomechanical mapping of normal and keratoconus corneas. JAMA Ophthalmol. 133 (4), 480–482. [PubMed: 25611213]

Scarcelli G, Besner S, Pineda R, Yun SH, 2014 Biomechanical characterization of keratoconus corneas ex vivo with Brillouin microscopy. Invest. Ophthalmol. Vis. Sci 55 (7), 4490–4495. [PubMed: 24938517]

Scarcelli G, Pineda R, Yun SH, 2012 Brillouin optical microscopy for corneal biomechanics. Invest. Ophthalmol. Vis. Sci 53 (1), 185. [PubMed: 22159012]

Scarcelli G, Yun SH, 2007 Confocal Brillouin microscopy for three-dimensional mechanical imaging. Nat. Photon 2, 39–43.

Thomasy SM, Raghunathan VK, Winkler M, Reilly CM, Sadeli AR, Russell P, Jester JV, Murphy CJ, 2014 Elastic modulus and collagen organization of the rabbit cornea: epithelium to endothelium. Acta Biomater. 10 (2), 785–791. [PubMed: 24084333]

White TL, Lewis PN, Young RD, Kitazawa K, Inatomi T, Kinoshita S, Meek KM, 2017 Elastic microfibril distribution in the cornea: differences between normal and keratoconic stroma. Exp. Eye Res 159, 40–48. [PubMed: 28315339]

Winkler M, Chai D, Kriling S, Nien CJ, Brown DJ, Jester B, Juhasz T, Jester JV, 2011a Nonlinear optical macroscopic assessment of 3-D corneal collagen organization and axial biomechanics. Invest. Ophthalmol. Vis. Sci 52 (12), 8818. [PubMed: 22003117]

Winkler M, Chai D, Kriling S, Nien CJ, Brown DJ, Jester B, Juhasz T, Jester JV, 2011b Nonlinear optical macroscopic assessment of 3-D corneal collagen organization and axial biomechanics. Invest. Ophthalmol. Vis. Sci 52 (12), 8818–8827. [PubMed: 22003117]

Winkler M, Shoa G, Xie Y, Petsche SJ, Pinsky PM, Juhasz T, Brown DJ, Jester JV, 2013 Three-dimensional distribution of transverse collagen fibers in the anterior human corneal stroma. Invest. Ophthalmol. Vis. Sci 54 (12), 7293–7301. [PubMed: 24114547]

Wu P-J, Kabakova I, Ruberti J, Sherwood JM, Dunlop IE, Paterson C, Török P, Overby DR, 2017 Brillouin microscopy, what is it really measuring? ArXiv e-prints 1711.

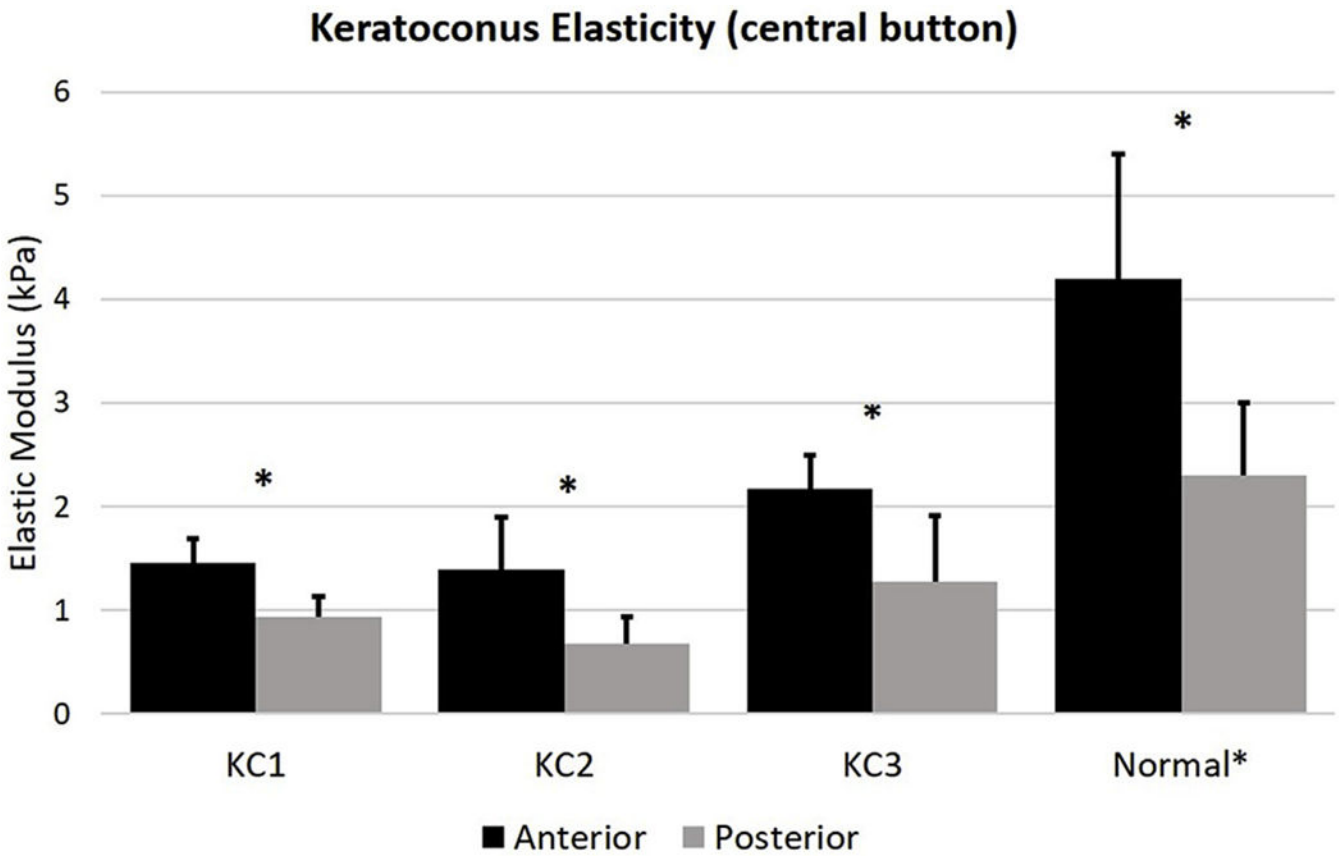

Fig. 1.

Elastic moduli in the anterior and posterior portions in keratoconic samples as measured by ARFEM. The anterior region is significantly stiffer than the posterior in all three samples. Elasticity data from a 2016 study in the healthy cornea has been included for comparison (Mikula et al., 2016). Asterisk (*) indicates significance ($p < 0.05$).

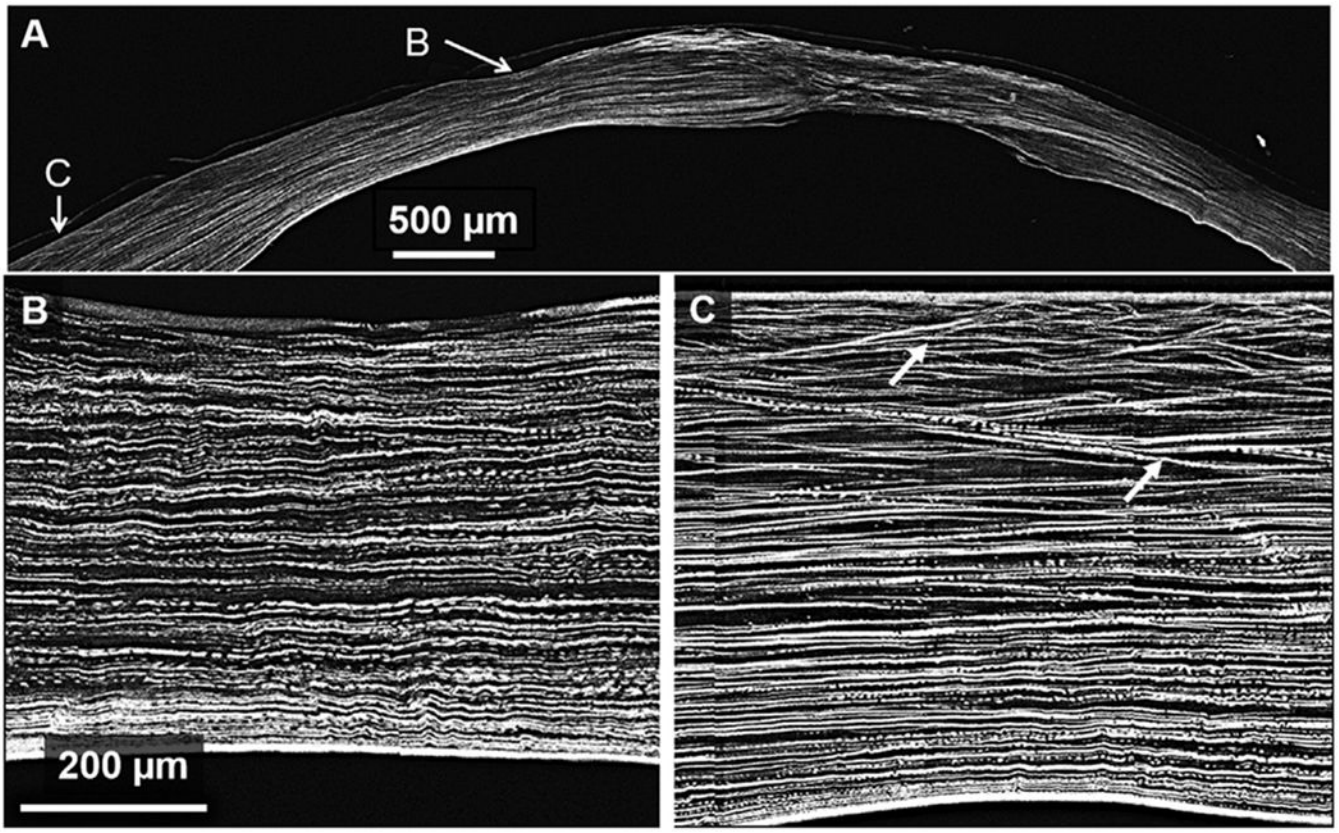

Fig. 2.

SHG backscatter image in a keratoconus cornea. Panel B is zoomed in on a region within the cone revealing a thin cornea with noticeably absent interweaving. Panel C is zoomed in on a region outside of the cone; anterior interweaving in this region is apparent as shown by lamellae forming acute angles to the corneal surface. White arrows indicate areas of branching.

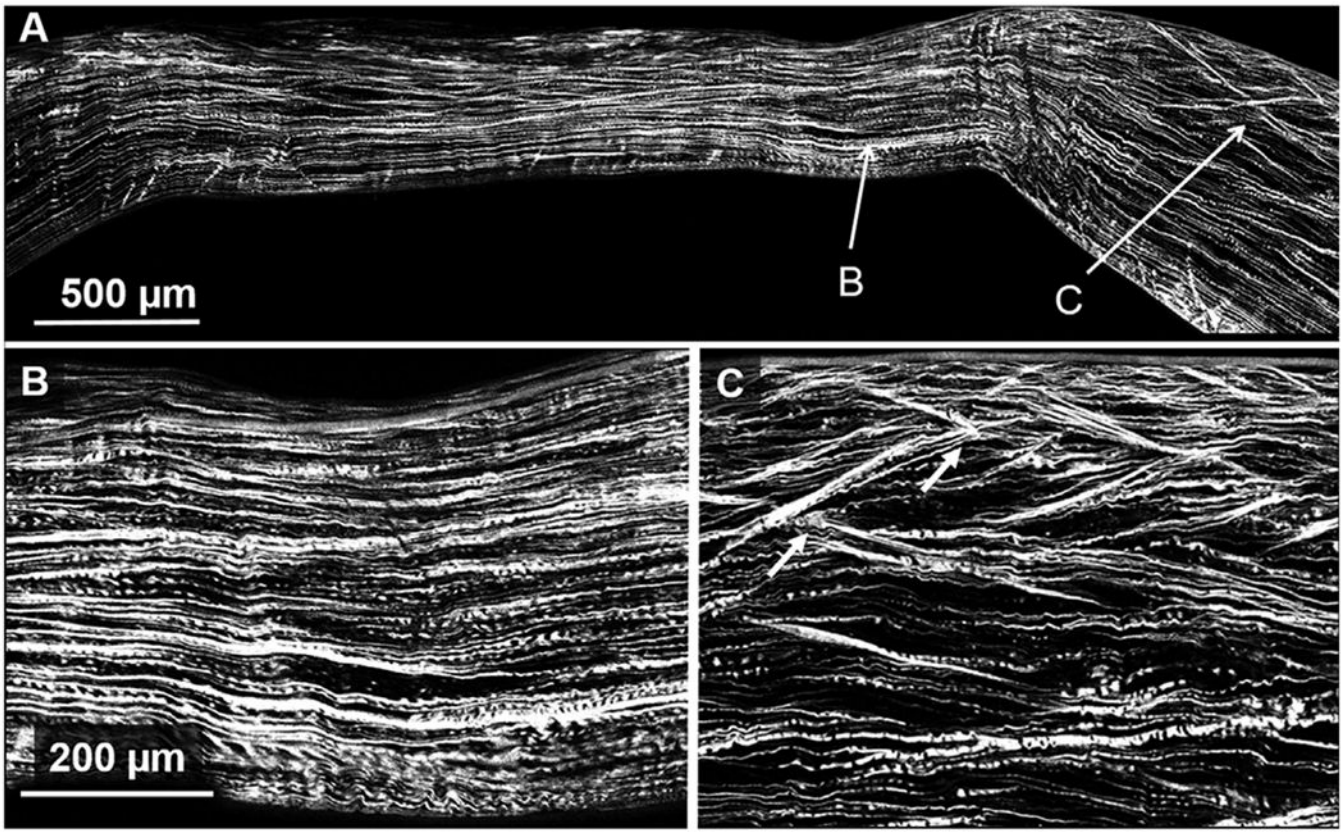

Fig. 3.

SHG backscatter image in a keratoconus cornea. Panel B is zoomed in on the thinnest region within the cone revealing a dearth of interweaving and breaks in Bowman's layer. Panel C is zoomed in on a region outside of the cone revealing normal looking structure and anterior interweaving as shown by lamellae forming acute angles to the corneal surface. White arrows indicate areas of branching.

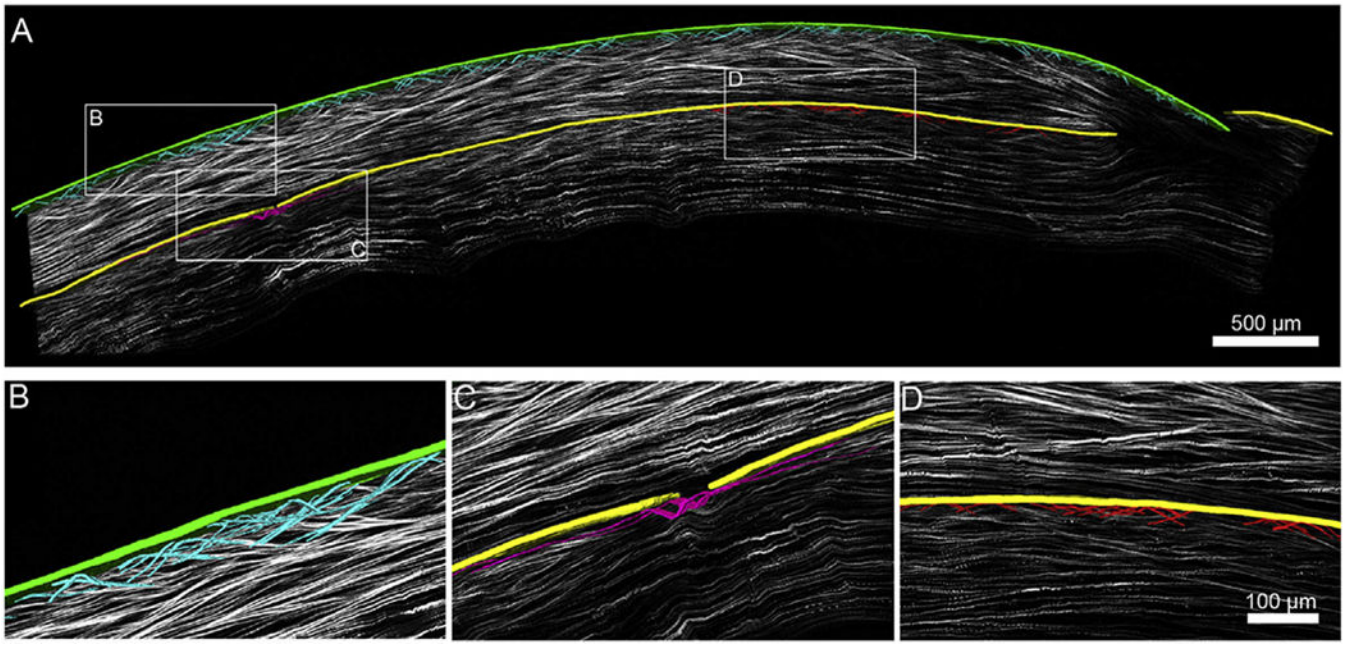

Fig. 4.

A. NLO HR-MAC image of a corneal cross section on a single optical plane out of 51 planes. Imposed on top of the single plane is a 3-D reconstruction of bow spring fibers (teal) inserting into Bowman's layer of the Epi-KP lenticule (green). Bow spring fibers (red) are shown inserting into Bowman's layer of the KC cornea (yellow) along with a single fiber (magenta) near the cone region. Fibers were segmented manually and rendered. Note: Image B,C,D are from different slices to show image at optimal resolution. B. Zoomed in 3-D reconstruction of a detailed fiber meshwork (teal) from the Epi-KP lenticule showing multiple branching points. C. Zoomed in 3-D reconstruction of a single fiber (magenta) running along the KC cornea near the cone region showing minimal branching compared to the Epi-KP lenticule in (B). Highlighted portion shows a break in Bowman's layer (yellow) and a lack of bow spring insertion. D. Zoomed in 3-D reconstruction of bow spring fibers (red) inserting into the KC Bowman's layer (yellow) along with a region of interweaving due to the significant distance from the cone (For interpretation of the references to colour in this figure legend, the reader is referred to the web version of this article).

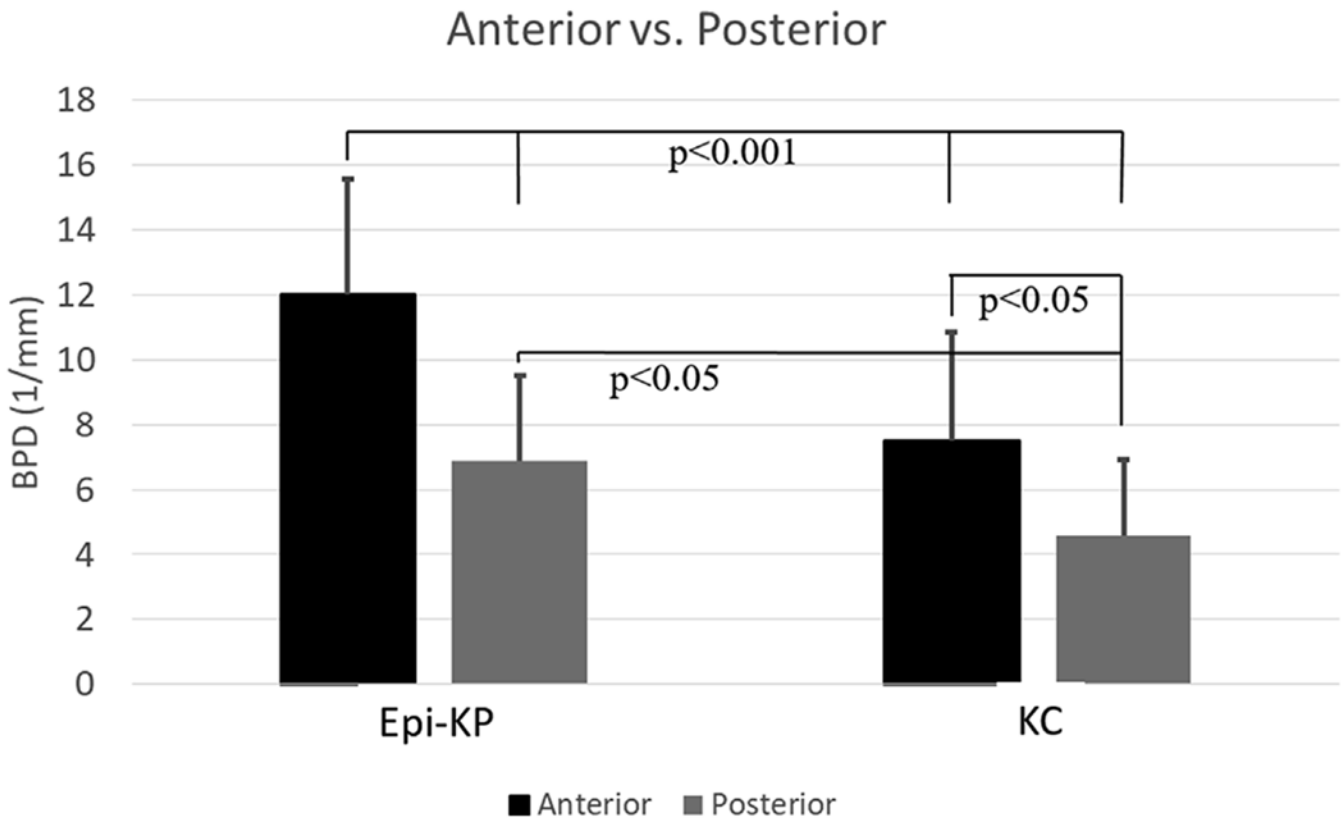

Fig. 5.

Branching point density (BPD) in the KC button and Epi-KP lenticule as a function of depth. The anterior and posterior are defined as being within 100 μm of the anterior and posterior surfaces of the region.

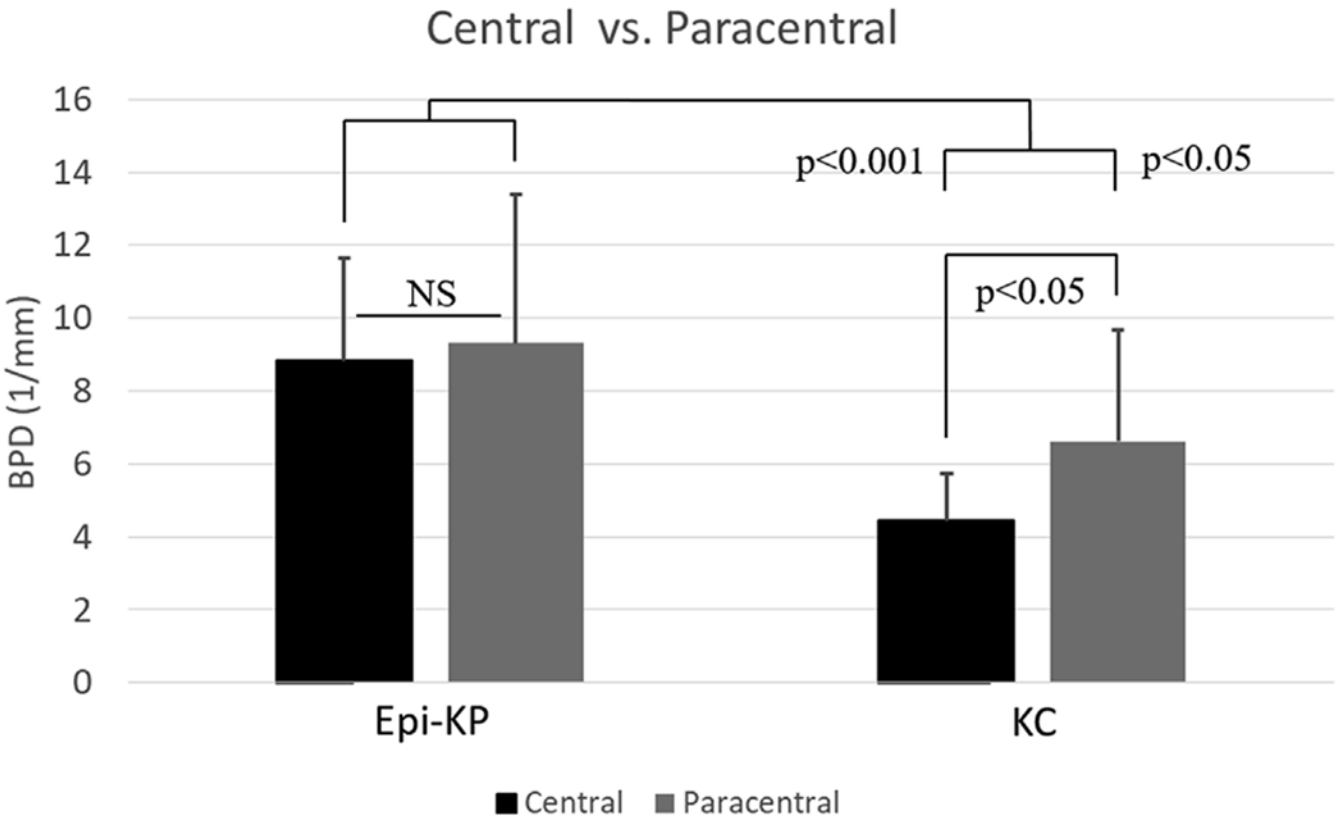

Fig. 6.

Branching point density (BPD) in the KC button and Epi-KP lenticule as a function of radial position (central vs. para-central).